Conductivity, weak ferromagnetism, and charge instability in an α-MnS single crystal

S. S. Aplesnin,* L. I. Ryabinkina, G. M. Abramova, O. B. Romanova, A. M. Vorotynov, D. A. Velikanov, N. I. Kiselev, and A. D. Balaev

Kirensky Institute of Physics, Siberian Branch of the Russian Academy of Sciences, Krasnoyarsk, 660036, Russia

(Received 16 April 2004; revised manuscript received 15 October 2004; published 15 March 2005)

The temperature dependence of resistivity, magnetization, and electron-spin resonance of the α-MnS single crystal were measured in temperature range of 5 K$<T<$550 K. Magnetization hysteresis in an applied magnetic field up to 0.7 T at $T=5$, 77, and 300 K, irreversible temperature behavior of magnetization, and resistivity were found. The obtained data were explained in terms of a degenerate tight binding model using random phase approximation. The contribution of holes in t_{2g} and e_g bands of manganese ions to the conductivity, optical absorbtion spectra, and charge instability in α-MnS were studied. Charge susceptibility maxima resulted from the competition of the on-site Coulomb interaction between the holes in different orbitals and small hybridization of subbands were calculated at $T=160$, 250, and 475 K.

DOI: 10.1103/PhysRevB.71.125204 PACS number(s): 71.45.Lr, 72.20.−i, 75.30.Cr, 75.60.Nt

I. INTRODUCTION

Recently the compounds with strong coupling of the charge-orbital and spin degrees of freedom have attracted extensive interest in connection with the specific property, namely the colossal magnetoresistance, i.e., the strong resistivity decrease in applied magnetic field.[1] In manganites with small concentration of doped carriers this strong coupling leads to ferromagnetism, which results from the competition between ferromagnetic double-exchange interaction and AFM super-exchange. High temperature behavior of the resistivity $\rho(T)$ in the manganites $R\mathrm{MnO_3}(R=\mathrm{La,Pr,Sm})$[2] looks like step function explained by the charge and orbital ordering. Since the substitution of manganese ion by another 3d-metal ion leads to the absence of these properties, the dramatic resistivity drop in applied magnetic field is attributed to the electronic state of the manganese ion.[3]

Similar effects have also been observed in compounds synthesized on basis of α-MnS. The diluted magnetic semiconductors $\mathrm{Mn_{(1-x)}Fe_xS}$ reveal the colossal magnetoresistance. The properties of these compounds should be caused by the electron structure of the manganese monosulfide, which results in a number of characteristic properties of MnS pure single crystals. Similar to $\mathrm{LaMnO_3}$, α-MnS sulfide shows antiferromagnetic (AF) ordering of the second kind consisted of ferromagnetically arranged spins in (111) plane and AF spin ordering along cube edges. Unlike $\mathrm{LaMnO_3}$ with Mn^{3+} ions, the ground state of the manganese ions in MnS with NaCl structure is Mn^{2+}. The resistivity of the MnS pure single crystals is independent of temperature at $T<T_N$ (Ref. 4) and behaves analogously to semiconductors up to 800 K. In temperature range of 400–550 K the resistivity of the manganese monosulfide has a plateau,[5] the mechanism of which is not studied yet. As the Hall effect measurements[5] showed, the conductivity is realized by holes in 3*d*-band of manganese ions.

The electronic and magnetic properties of α-MnS have been studied in the framework of the density functional level theory by self-consistent solving the Kohn-Sham equation.[6] First principle calculations confirm the hole character of the conductivity. The e_g and t_{2g} bandwidths of Mn states are $\sim$2.5 eV and $\sim$1 eV, respectively. The t_{2g} bands corresponding to the spin-up and spin-down electron states are separated by $\sim$1.6 eV. The Fermi level is located at the bottom of the t_{2g} band with the spin down. The states of the valence band are occupied by electrons of both *p* sulfur and *d* manganese orbitals and the gap value is $\sim$1.5 eV.

In this paper we determine the contribution of the carriers in the upper e_g and t_{2g} Hubbard bands to the conductivity at low and high temperatures and the influence of charge instability on the transport and magnetic properties of α-MnS. In contrast to manganite, the weak magnetic moment results from the orbital moment ordering the holes localized in one of the subbands t_{2g}.

II. EXPERIMENTAL RESULTS

The α-MnS single crystal was made by liquid manganese saturation with sulfur at $T\sim$1245 °C. X-ray diffraction analysis was performed on DRON-2.0 diffractometer with the monochromatic CuKα radiation at temperatures of 80–300 K. The resistance measurements were made in [111] and [100] directions at temperatures of 90–550 K. The fluorescence spectroscopy experiment was carried out on SPARK-1 spectrometer. According to the x-ray analysis data, the synthesized α-MnS sample is the single crystal, which has a NaCl cubic lattice with the cell parameter $a=5.22$ Å. In Fig. 1 the temperature dependence of the resistivity ρ for the α-MnS single crystal is shown. One can clearly see a gradual change of the resistivity during the sample heating several times up to 550 K. The first heating-and-cooling cycle causes significant temperature hysteresis $\Delta\rho/\rho\sim1$ and the second cycle yields $\Delta\rho/\rho\sim0.2$ at $T=280$ K. During the subsequent heating-and-cooling cycles the temperature hysteresis of the resistivity disappears, and the resistivity has a plateau in the range of 420–550 K, showing good agreement with the previously obtained data.[5] These measurements were made at high vacuum and the results appeared reproducible after long keeping at room temperature.

The current-voltage characteristic shows the small negative differential conductivity at $U=2$ and 30 V and T

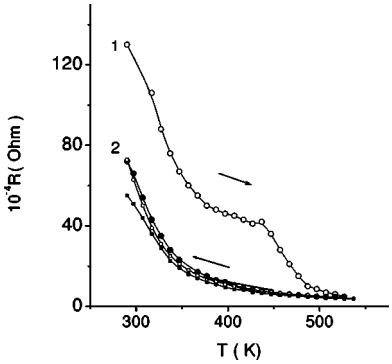

FIG. 1. The temperature dependence of the resistivity measured at two cycles of heating and cooling: the first (1) and the second (2) cycles.

=280 K, which disappears at $T=550$ K. The dI/dU curves are presented in Fig. 2. The behavior of $\rho(U)$ at $T=560$ K is typical for semiconductors. The magnetic susceptibility measured in range of 77 K$<T<$300 K is nonlinear at low magnetic fields $H=200$ and 1000 Oe with anisotropy value $\Delta\chi/\chi$ along the [100] and [111] directions of $\sim$0.16, and correlates with the anisotropy resistivity $(1-\rho_{[100]}/\rho_{[111]})\sim 0.46$.[4]

Magnetization measurements were carried out with the superconducting quantum interference device (SQUID magnetometer). Specimens were cooled to 5 K and then heated to the highest temperature in zero magnetic field. The monocrystal was found to have a small spontaneous moment in the range of 4.2–300 K. The $m(T)$ curves for [001] and [111] are shown in Fig. 3. After cooling of α-MnS in magnetic field $H=200$ Oe magnetization $m_{[111]}(T)$ exhibits qualitatively different temperature dependence. Magnetization vs H curves at $T=5$, 77, and 300 K are presented in Fig. 4.

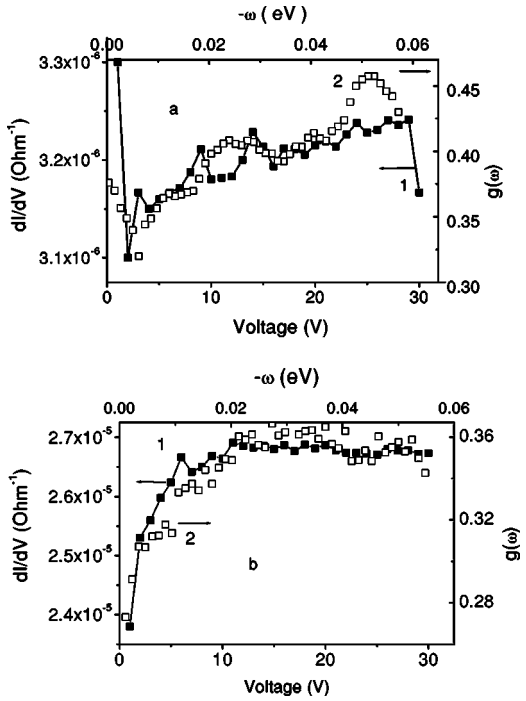

FIG. 2. The voltage derivative of current $dI/dV(1)$ and density of state near the chemical potential $g(\omega)(2)$ at (a) $T=280$ K and (b) 550 K.

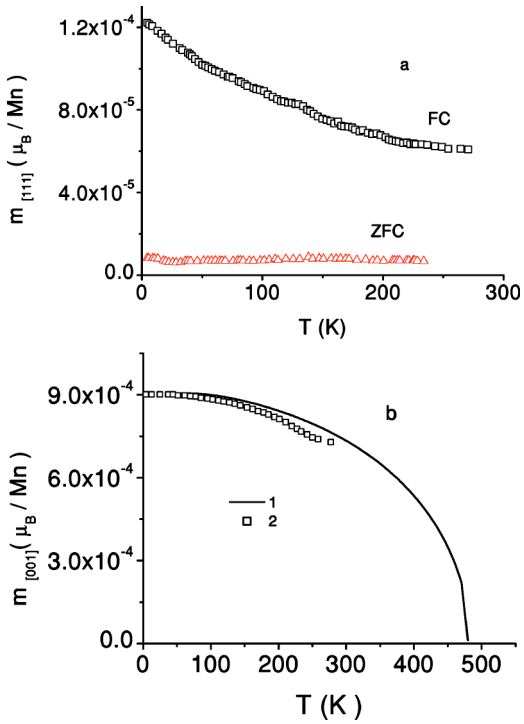

FIG. 3. The temperature dependence of the residual magnetization on the one manganese ion along [111] (a) measured in zero field cold (ZFC) and at $H=200$ Oe (FC). Estimated (1) by Eq. (11) and measured (2) magnetization along [001] versus temperature (b).

Electronic spin resonance (ESR) measurements were performed with the X-band Radiopan SE/X-2544 spectrometer at $\nu\simeq 9.4$ GHz(150 K$<T<$300 K), using a continuous gas-flow cryostat for N_2. The oriented sample was placed into a quartz tube. Figure 5 shows the temperature dependences of the ESR linewidth ΔH and the effective g value $g_{eff}=h\nu/(\mu_B H_{res})$ determined from H_{res}. The largest difference between the linewidths $\delta H=\Delta H_{[001]}-\Delta H_{[100]}$ along [001] and [100] is observed near the rhombohedral lattice deformation. The δH value changes a sign at $T\simeq 250$ K. The g-values show a small increase at $T>200$ K and approach high-temperature value. The zero-field splitting parameters

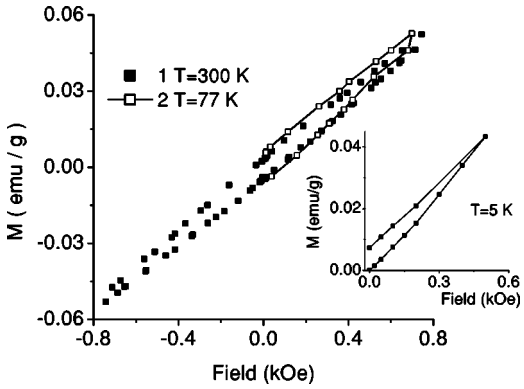

FIG. 4. The magnetization vs. magnetic field at the different temperatures.

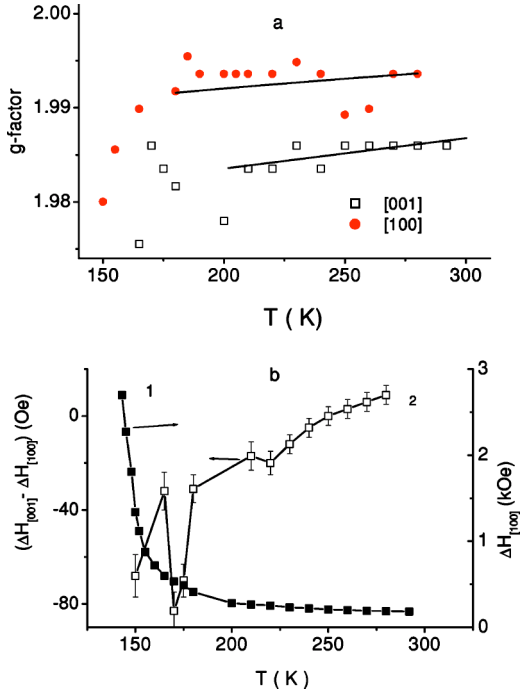

FIG. 5. The temperature dependence of (a) the effective g value $g_{eff}(T)$ and (b) ΔH (1), $\Delta H_{[001]} - \Delta H_{[100]}$ (2) for H parallel to the crystallographic axis. Solid lines represent the fits using Eq. (12) for g_{eff}.

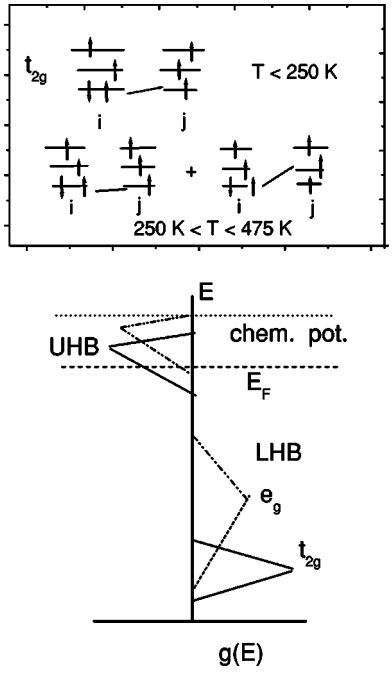

FIG. 6. Schematic drawing of the t_{2g} holes moving on the sites and density of states of single electron excitations in the t_{2g} (solid) and e_g (dotted) lower Hubbard band (LHB) and upper Hubbard band (UHB) with arrangement of Fermi level (E_F) and chemical potential (Ref. 6).

(D and E is the axial and rhombic terms of the single ion anisotropy) can be determined from the temperature dependence of H_{res} using the general formula for the resonance shift that resulted from the crystal field as will be shown below.)

III. MODEL AND CALCULATION METHOD

The covalent bond between sulphur and manganese ions leads to redistribution of the electron density on these ions. The sulphur electrons locate on the Mn^{2+} ion. An addition of the $d^6(t_{2g}^4 e_g^2)$ term to the main term of d^5 corresponds to partial filling of the upper Hubbard band. A schematic image of the electron density of states of manganese ions calculated by Taperro *et al.*[6] is shown in Fig. 6. The Fermi level locates below the chemical potential at the bottom of the upper Hubbard band. We neglect the e_g and t_g bands hybridization and thus, the conductivity can be estimated as an additive quantity of $\sigma = \sigma_{e_g} + \sigma_{t_{2g}}$. Schematic representation of the charge transport through the lattice sites is shown in Fig. 6. Electrostatic interaction of excess charge lifts the double and triple degeneration of the e_g and t_{2g} subbands in the cubic crystal and causes the rhombohedral deformation of the lattice with the local symmetry breaking. According to ESR measurements, the anisotropy of g value at $T > 170$ K is $\delta g/g \simeq 0.99$ and local deformations lead to a small difference of values of hopping integrals parameters along directions [100], [010], [001], which is $\delta t/t \sim (\delta g/g)^{1/4} \sim 0.998$. We neglect this difference and consider the isotropic case.

Theoretical analysis was made in terms of the degenerate tight-binding model with three interaction parameters: the direct Coulomb integral between the different orbital electrons U and the intraband and interband hopping matrix elements. Interorbital exchange J is much less than Coulomb interaction $J/U \sim 0.2$ and may be omitted. The motion of the charge carriers is considered in the paramagnetic phase with the small holes concentration. According to Hall measurements the charge carriers have the hole type of the conductivity. Below we will show that the averaged group velocity and excitation spectrum on the Fermi surface in our model have different from typical electron excitations in metals sign and are similar to doped nondegenerate semiconductors. The holes concentration can be estimated from bandwidth value $W_t \sim 1$ eV and the charge transfer gap calculated from the well-known relation $E_g = \epsilon_p - \epsilon_d + U_{dd}$, where $\epsilon_{p,d}$ are the atomic orbital eigenvalues, on the levels p, d for sulphur and for manganese ions, and U_{dd} is the intraatomic Coulomb parameter within the same orbital. The Coulomb integral is estimated from the difference of energies E^+ and E^{3+} for $d^6(4t_{2g}2e_g)$ and $d^4(2t_{2g}2e_g)$. The relations $\Omega_1 = E^{3+} - E^{2+}$ and $\Omega_2 = E^+ - E^{2+}$ are found from x-ray photoelectron spectra[5] and are equal to $\Omega_1 \sim -1.5$ eV, $\Omega_2 \sim 1.5$ eV, and $U_{dd} = \Omega_2 - \Omega_1 \sim 3$ eV. The value $\epsilon_p - \epsilon_d \sim 1$ eV is equal to the difference of energies corresponding to maximum of DOS on $3P$ sulphur and $d^5 t_{2g}$ manganese ions.[6] The concentration is proportional to the hybridization degree $n \sim (W_t/zE_g)^2$, which is equal to $n \simeq 5 \times 10^{-3}$ and 0.01 for t_{2g} and e_g states, respectively. The first principles calculations[6] give the higher value of the concentration $n(t_{2g}) \simeq 0.03$, $n(e_g) \simeq 0.07$. The appearance of two electrons on the d-level causes the reduction of the manganese ion spin $S = 4.4\mu_B$.[6]

Below we consider the motion of charged carriers only in the upper Hubbard band in the frame of the effective model

with the spinless fermions. The model Hamiltonian is described as follows:

$$H_t = -\sum_{i,j,\alpha} t_{i,j}^{\alpha\alpha} a_{i\alpha}^{+} a_{j\alpha} - \sum_{i,j,\alpha>\beta} t_{i,j}^{\alpha\beta} a_{i\alpha}^{+} a_{j\beta} - \mu n + \sum_{i,\alpha>\beta} U n_{i\alpha} n_{i\beta},$$

$$H_e = -\sum_{i,j,\alpha} t_{i,j}^{\alpha\alpha} c_{i\alpha}^{+} c_{j\alpha} - \sum_{i,j,\alpha>\beta} t_{i,j}^{\alpha\beta} c_{i\alpha}^{+} c_{j\beta} - \mu n + \sum_{i,\alpha>\beta} U n_{i\alpha} n_{i\beta}, \tag{1}$$

where $a_{i\alpha(\beta)}$ is the annihilation operator of the $t_{2g,\alpha(\beta)}$, the orbital holes $[\alpha(\beta)=xy,yz,zx]$; $c_{i\alpha(\beta)}$ is the annihilation operator of the $e_{g,\alpha(\beta)}$, the orbital holes $[\alpha(\beta)=x^2-y^2,3z^2-r^2]$, μ is the chemical potential, n is the holes concentration, and $t_{i,j}^{\alpha\alpha}$ is the hopping integral.

Let us write the system of three equations for the Green's functions describing the hole motion in t_{2g} band. When using random phase approximation, the equation sets for the Green's functions $\langle\langle a_{\mathbf{r},\alpha} | a_{\mathbf{r},\alpha}^{+}\rangle\rangle$ and $\langle\langle a_{\mathbf{r},\alpha} | a_{\mathbf{r},\alpha}^{+}\rangle\rangle$ are being closed. These equations have the following form:

$$(\omega - E_{\mathbf{k}}^{\alpha}) G_{\mathbf{k}}^{\alpha\alpha} + \varepsilon_{\mathbf{k}} G_{\mathbf{k}}^{\beta\alpha} + \varepsilon_{\mathbf{k}} G_{\mathbf{k}}^{\beta'\alpha} = 1,$$

$$\varepsilon_{\mathbf{k}} G_{\mathbf{k}}^{\alpha\alpha} + (\omega - E_{\mathbf{k}}^{\beta}) G_{\mathbf{k}}^{\beta\alpha} + \varepsilon_{\mathbf{k}} G_{\mathbf{k}}^{\beta'\alpha} = 0,$$

$$\varepsilon_{\mathbf{k}} G_{\mathbf{k}}^{\alpha\alpha} + \varepsilon_{\mathbf{k}} G_{\mathbf{k}}^{\beta\alpha} + (\omega - E_{\mathbf{k}}^{\beta'}) G_{\mathbf{k}}^{\beta'\alpha} = 0,$$

$$G_{\mathbf{k}}^{\alpha\alpha} = \langle\langle a_{\mathbf{k},\alpha} | a_{\mathbf{k},\alpha}^{+}\rangle\rangle,$$

$$G_{\mathbf{k}}^{\beta(\beta')\alpha} = \langle\langle a_{\mathbf{k},\beta(\beta')} | a_{\mathbf{k},\alpha}^{+}\rangle\rangle,$$

$$E_{\mathbf{k}}^{\alpha} = \varepsilon_{\mathbf{k}}^{\alpha} - \mu + U(n_{\beta} + n_{\beta'}),$$

$$E_{\mathbf{k}}^{\beta(\beta')} = \varepsilon_{\mathbf{k}}^{\beta(\beta')} - \mu + U(n_{\alpha} + n_{\beta'(\beta)}),$$

$$\varepsilon_{\mathbf{k}}^{\alpha(\beta)} = -4t_{xy}\cos\frac{k_x}{2}\cos\frac{k_y}{2} - 4t_{xz}\cos\frac{k_x}{2}\cos\frac{k_z}{2} - 4t_{zy}\cos\frac{k_z}{2}\cos\frac{k_y}{2} - 2t_x\cos k_x - 2t_y\cos k_y - 2t_z\cos k_z,$$

$$\varepsilon_{\mathbf{k}} = -2t(\cos k_x + \cos k_y + \cos k_z),$$

$$n = n_1 + n_2 + n_3. \tag{2}$$

The values $\varepsilon_{\mathbf{k}}^{\alpha}$ have a different set of hopping integral parameters $\alpha=xy$, $t_{xy} \gg t_{yz}$, t_{xz}, $\alpha=yz$, $t_{yz} \gg t_{xz}$, t_{xy}, $\alpha=xz$, $t_{xz} \gg t_{yz}$, t_{xy}. The equation set for the Green's functions $\langle\langle c_{\mathbf{r},\alpha} | c_{\mathbf{r},\alpha}^{+}\rangle\rangle$ and $\langle\langle c_{\mathbf{r},\alpha} | c_{\mathbf{r},\beta}^{+}\rangle\rangle$ describing the carriers dynamic in the e_g subbands has the following form:

$$(\omega - A_{\mathbf{k}}^{\alpha}) G_{\mathbf{k}}^{\alpha\alpha} + \varepsilon_{\mathbf{k}} G_{\mathbf{k}}^{\beta\alpha} = 1,$$

$$\varepsilon_{\mathbf{k}} G_{\mathbf{k}}^{\alpha\alpha} + (\omega - A_{\mathbf{k}}^{\beta}) G_{\mathbf{k}}^{\beta\alpha} = 0,$$

$$G_{\mathbf{k}}^{\alpha\alpha} = \langle\langle c_{\mathbf{k},\alpha} | c_{\mathbf{k},\alpha}^{+}\rangle\rangle; \quad G_{\mathbf{k}}^{\beta\alpha} = \langle\langle c_{\mathbf{k},\beta} | c_{\mathbf{k},\alpha}^{+}\rangle\rangle,$$

$$A_{\mathbf{k}}^{\alpha(\beta)} = \varepsilon_{\mathbf{k}}^{\alpha(\beta)} - \mu + U n_{\beta(\alpha)},$$

$$\varepsilon_{\mathbf{k}}^{\alpha(\beta)} = -2t_x^{\alpha}\cos k_x - 2t_y^{\alpha}\cos k_y - 2t_z^{\beta}\cos k_z,$$

$$\varepsilon_{\mathbf{k}} = -2t(\cos k_x + \cos k_y + \cos k_z). \tag{3}$$

The type of $\varepsilon_{\mathbf{k}}^{\alpha(\beta)}$, $\alpha=x^2-y^2$, $\beta=3z^2-r^2$, reflects the symmetry of the *sp* wave function's hybridization of the sulphur ion with the $d_{x^2-y^2}$, $d_{3z^2-r^2}$ wave functions.

The solution of Eq. (2) is reduced to the following cubic equation for determining of the excitation spectrum:

$$\omega^3 - A\omega^2 + B\omega + A\varepsilon_{\mathbf{k}}^2 + 2\varepsilon_{\mathbf{k}}^3 - E_{\mathbf{k}}^{xy} E_{\mathbf{k}}^{xz} E_{\mathbf{k}}^{yz} = 0,$$

$$A = E_{\mathbf{k}}^{xy} + E_{\mathbf{k}}^{xz} + E_{\mathbf{k}}^{yz}, \tag{4}$$

$$B = E_{\mathbf{k}}^{xy} E_{\mathbf{k}}^{xz} + E_{\mathbf{k}}^{xy} E_{\mathbf{k}}^{yz} + E_{\mathbf{k}}^{xz} E_{\mathbf{k}}^{yz} - 3\varepsilon_{\mathbf{k}}^2.$$

The excitation spectrum in e_g subbands is found from Eq. (3):

$$\omega_{1,2}(k) = \tfrac{1}{2}(A_{\mathbf{k}}^{\alpha} + A_{\mathbf{k}}^{\beta} \pm \sqrt{(A_{\mathbf{k}}^{\alpha} - A_{\mathbf{k}}^{\beta})^2 + 4\varepsilon_{\mathbf{k}}^2}). \tag{5}$$

The chemical potential is calculated from the self-consistent equation for the hole concentration n:

$$n = \frac{1}{N}\sum_{\mathbf{k},\alpha} \int d\omega f(\omega) \frac{1}{\pi} \operatorname{Im} G^{\alpha\alpha}(\mathbf{k}\omega), \tag{6}$$

where $f(\omega)=[\exp(\omega/T)+1]^{-1}$. The summation over the momentum in the Brillouin zone is made using $8\cdot 10^6$ points. The holes distribution function in e_g and t_{2g} subbands is calculated by this expression:

$$N(\mathbf{k}) = \int d\omega f(\omega) \frac{1}{\pi} \operatorname{Im} G^{\alpha\alpha}(\mathbf{k}\omega),$$

$$N_e^{\alpha}(\mathbf{k}) = \frac{A_{\mathbf{k}}^{\alpha}(f(\omega_2) - f(\omega_1)) + \omega_1 f(\omega_1) - \omega_2 f(\omega_2)}{\omega_1 - \omega_2},$$

$$N_t^{\alpha}(\mathbf{k}) = f(\omega_1)\frac{\varepsilon_{\mathbf{k}} - (\omega_1 - E_{\mathbf{k}}^{\beta})(\omega_1 - E_{\mathbf{k}}^{\beta'})}{(\omega_1 - \omega_2)(\omega_1 - \omega_3)} + f(\omega_2)\frac{\varepsilon_{\mathbf{k}} - (\omega_2 - E_{\mathbf{k}}^{\beta})(\omega_2 - E_{\mathbf{k}}^{\beta'})}{(\omega_2 - \omega_3)(\omega_2 - \omega_1)} + f(\omega_3)\frac{\varepsilon_{\mathbf{k}} - (\omega_3 - E_{\mathbf{k}}^{\beta})(\omega_3 - E_{\mathbf{k}}^{\beta'})}{(\omega_3 - \omega_2)(\omega_3 - \omega_1)}, \tag{7}$$

where ω_i are determined from Eqs. (4) and (5). Holes concentrations in subbands (n_1, n_2) are found by minimization of the grand canonical potential of the holes gas:

$$\frac{\partial U_g}{\partial n_1} + \frac{\partial U_g}{\partial n_2} = 0,$$

$$U_g = \frac{1}{N}\sum_{\mathbf{k},\alpha} [\omega(\mathbf{k}) f(\omega(\mathbf{k})) - k_B T f(\omega(\mathbf{k}))\ln f(\omega(\mathbf{k}))] - \mu n. \tag{8}$$

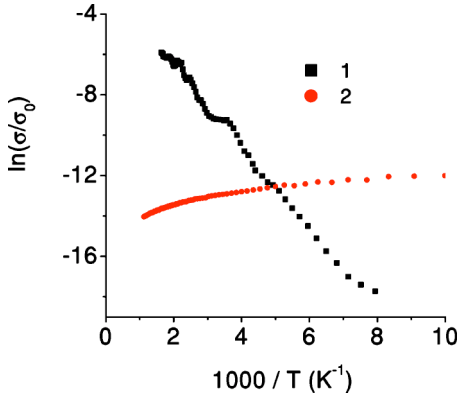

FIG. 7. The temperature dependence of the hole conductivity in $t_{2g}(1)$ and in $e_g(2)$ bands normalized to the constant σ_0 defining the dimension of conductivity.

The transport properties such as a conductivity can be obtained from Kubo formula in the limit of $d \to \infty$ (Ref. 7):

$$\sigma(\omega) = \sigma_0 \sum_{\alpha} \int d\omega' I_{\alpha}(\omega', \omega' + \omega) \frac{f(\omega') - f(\omega' + \omega)}{\omega},$$

$$I_{\alpha}(\omega_1, \omega_2) = \frac{1}{\pi^2} \sum_{\mathbf{k}} \mathrm{Im}\, G_{\alpha}(\mathbf{k}, \omega_1) \mathrm{Im}\, G_{\alpha}(\mathbf{k}, \omega_2), \qquad (9)$$

where σ_0 is a constant defining the conductivity dimension. In order to estimate U Coulomb potential, we used the relation between intra- and interband Coulomb parameter $U'/U \sim 0.6$ determined on the basis of the first principles calculation method for the perovskite compounds.[8] To achieve the best agreement between the theoretical results and the experimental data, such as the temperature dependence of resistivity, the activation energy, the current derivative of voltage, and the optical absorption spectrum, we obtained the values for the following parameters $(t_x, t_y, t_z, t_{xy}, t_{xz}, t_{yz})$ used in Eq. (2) $(0.4, 0.4, 0.04, 1, 0.1, 0.1)t_0$, $(0.4, 0.04, 0.4, 0.1, 1, 0.1)t_0$, and $(0.04, 0.4.0.4, 0.1, 0.1, 1)t_0$, $t_0 = 0.067$ eV for d_{xy}, d_{yz}, d_{zx} orbitals, respectively, and (t_x, t_y, t_z) used in Eq. (3) $(0.1, 0.1, 1)t_0$ and $(1, 1, 0.1)t_0$, $t_0 = 0.11$ eV for $(3z^2 - r^2)$ and $(x^2 - y^2)$ orbitals, respectively. These bands are occupied by holes with the average filling numbers $n_t = 0.015$ and $n_e = 0.04$. The Coulomb integral between different electron orbitals is $U = 2$ eV. The hybridization of subbands may result from the electron-phonon interaction or interaction of different orbitals via anion with effective hopping parameter $t = 0.05t_0$.

IV. DISCUSSION

Calculated optical conductivity $\sigma(\omega)$ for the e_g band reveals the optical quasigap at $\omega = 0.28$ eV. The temperature dependence of the normalized conductivity $\sigma(\omega \to 0)$ calculated at $\omega \simeq 10^{-4}$ eV is presented in Fig. 7. The conductivity realized by the carriers in the e_g band decreases with the temperature increase, similar to an electron gas in metals.

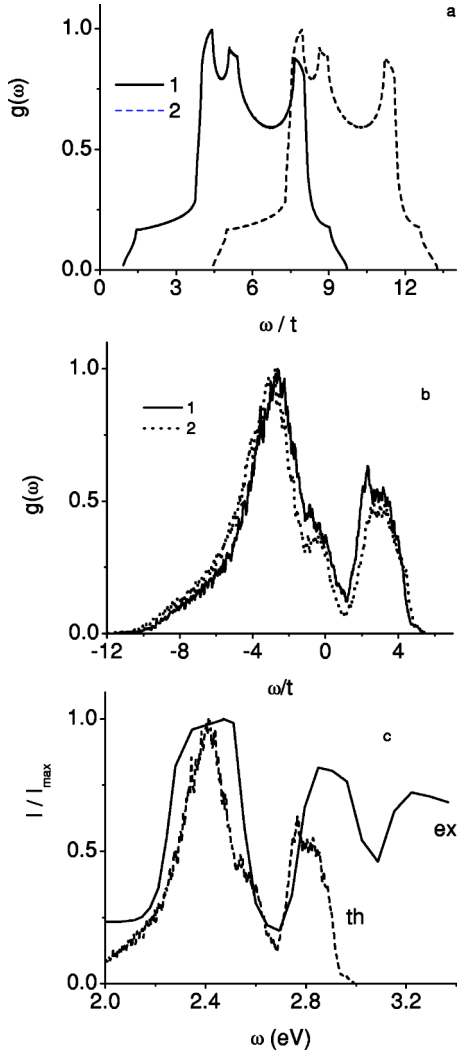

FIG. 8. The density of states $g(\omega)$ of single particle excitations in e_g band at (a) $T = 100$ K(1), 400 K(2) and in t_{2g} band at (b) $T = 200$ K(1), 700 K(2) where energy is normalized to hopping parameter t. The optical absorbtion spectrum measured in Ref. 9 (solid line) at $T = 170$ K and the calculated density of states of holes in t_{2g} band (dotted line).

The small $\sigma(T)$ value results from Coulomb gap Δ_c at the Fermi level. The $\Delta_c = E_F - \mu$ dependence on temperature fits well the linear $(E_F - \mu) \simeq 11T$. The typical temperature dependence of resistivity for semiconductors is $\rho \sim \rho_0 \exp(\Delta_c/T)$ and $\rho \sim \rho_0 \exp(11)$ for the α-MnS at $T < T_N$. The resistivity is independent of temperature, which is in good agreement with the experiment.

The conductivity of the t_{2g} band is attributed to the thermally activated carriers. Chemical potential lies in the range of energies between two peaks forming the effective quasigap in the excitation spectrum, as shown in Fig. 8(b). As one can see from Fig. 7, the holes in the e_g and t_{2g} bands make the main contribution to the conductivity at $T < 200$ K and at $T > 200$ K, respectively.

Calculated resistivity $\rho = 1/\sigma, \sigma = \sigma_t + \sigma_g$, is presented in Fig. 9. Good agreement with the experimental data obtained for the α-MnS single crystal is observed. In Fig. 9 ρ is nor-

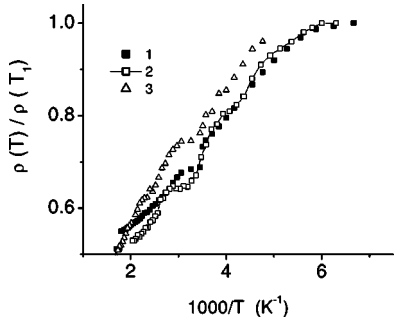

FIG. 9. The temperature dependence of resistivity measured (1) and calculated for $n_\alpha = n, n_\beta = 0(2), n_1 = n_2 = n_3 = n/3(3)$ normalized to the resistivity value at $T_1 = 166$ K.

malized to the resistivity $\rho(T_1)$, where $T_1 = 166$ K corresponds to rhombohedral lattice distortion temperature. The estimated and measured values of the activation energy are equal to $E_a \simeq 0.2$ eV. Sharp resistivity decrease at $T \sim 300$ K arises from partial lifting of the degeneracy of xy, xz, zy subbands. Minimization of the grand canonical potential of the holes gas U with respect to the average filling number gives the values of $n_\alpha \simeq n$ and $n_\beta = n_{\beta'} \to 0$ at $T < 250$ K and uniform filling subbands at $T > 475$ K.

To understand the moving of charge carriers in the magnetic field we calculate the averaged group velocity on the Fermi surface. The excitation spectra along three directions are shown in Fig. 10. The large interdot space near the chemical potential results from using the discrete number of the wave vectors in Brillouin zone. The group velocity on the Fermi surface $\nabla_{\mathbf{k}}\omega(\mathbf{k}) < 0$ and the acceleration of charge carriers in the magnetic field differs in sign as compared to the electrons in metals $\nabla_{\mathbf{k}}\omega(\mathbf{k}) > 0$. Such excitations are similar to the hole excitations.

The conductivity is proportional to the velocity and density of the charge carriers number N_μ at the chemical potential. The filling numbers distribution function $N(\mathbf{k})$ has maxima at the chemical potential. The temperature dependence of $N_{max}(\mathbf{k})$ reveals the remarkable slope changes at definite temperatures (Fig. 11), which correlates with the peculiarities of the conductivity temperature dependence. The calculation of $N_{max}(\mathbf{k})$ allows us to determine the wave vector of the charge ordering. So, the charge susceptibility is calculated as

$$\chi_c = dn/d\mu = \sum_{\mathbf{k}} \frac{dN(\mathbf{k})}{d\mathbf{k}} \frac{d\mathbf{k}}{d\mu} \sim \sum_{\mathbf{km}} \frac{dN(\mathbf{km})}{d\mathbf{km}} \frac{d\mathbf{km}}{d\mu}$$

(where summation over **km** is made near the chemical potential). The width of distribution $N(\mathbf{k})$ near N_{max} is characterized by the dispersion $D(\mathbf{q}) = \Sigma_{\mathbf{k}} N(\mathbf{k}) N(\mathbf{k}+\mathbf{q}) - \langle N \rangle^2$. At low temperatures the high D value arises from the multipeaks structure of $N(\mathbf{k})$. At high temperatures D increases as a consequence of the Fermi function broadening on the chemical potential. The filling numbers distribution function $N(\mathbf{k})$ has several maxima N_{max} at different wave vectors $\mathbf{k}_{\mathbf{m},\mathbf{i}}$ with the same excitation energies. The temperature dependencies of N_{max}, $\mathbf{k}_{\mathbf{m}}$ values and the difference of the wave

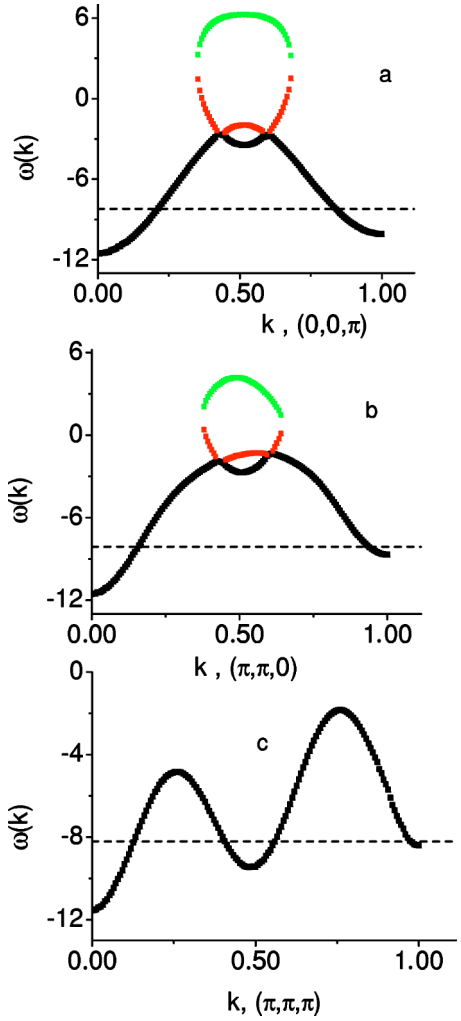

FIG. 10. The excitation spectrum in t_{2g} band along (a) [001], (b) [110], and (c) [111]. Fermi level is denoted by the dotted line.

vectors $\Delta\mathbf{k}_{\mathbf{m}} = \mathbf{k}_{\mathbf{m}1} - \mathbf{k}_{\mathbf{m}2}$ corresponding to two N_{max} are shown in Fig. 11. There are two transitions associated with the change of the wave vector $\mathbf{k}_{\mathbf{m}1}$ at $T = 250$ K and at $T = 475$ K. The change of $\mathbf{k}_{\mathbf{m}2}$ with respect to $\mathbf{k}_{\mathbf{m}1}$ is observed in the xy plane at $T < 300$ K. At $T > 475$ K the distribution function $N(\mathbf{k})$ has only one maximum. The maximal value of $D(\mathbf{q}_{\mathbf{m}})$ together with the wave vector q_m are shown in Fig. 12. The dispersion minimum is reached at $T = 475$ K. The essential change of q_m is observed in temperature range $400\ \text{K} < T < 470$ K. The relaxation time τ of the current carriers is dependent on the hole wave number that should lead to the conductivity anisotropy. The charge susceptibility of the holes $\chi_c = dn/d\mu$ in the t_{2g} band reveals two maxima at the temperatures $T = 250$ K and $T = 475$ K (see Fig. 13). The inverse value $1/\chi_c$ in e_g band reaches minimum at $T \simeq 160$ K near the temperature of the transition ($T_1 = 166$ K) attributed to the rhombohedral deformation of the lattice.

The resistivity value with uniform distribution of the average filling number in subbands d_{xy}, d_{xz}, d_{yz} is more than the resistivity of system with one partially filled subband at $T < 500$ K (Fig. 9). This is in qualitative agreement with the experimental data obtained at heating of the α-MnS single

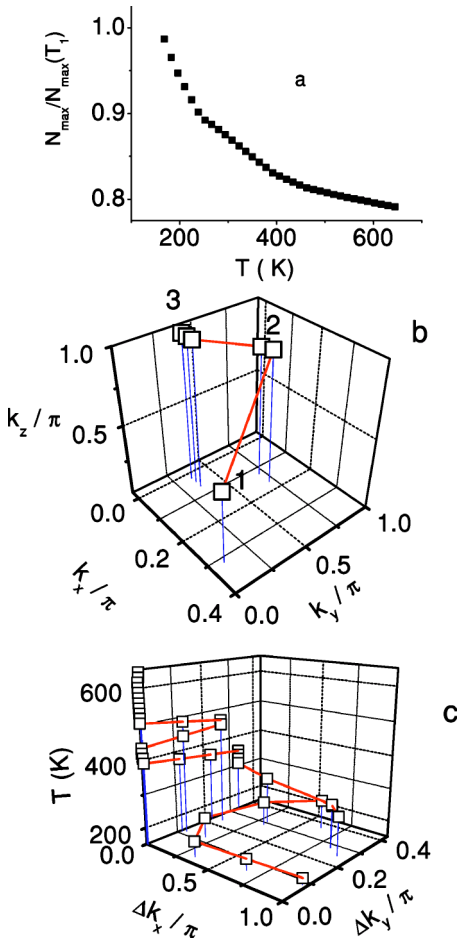

FIG. 11. The distribution function maximum of holes filling numbers (a) $N_{max}(\mathbf{k})/N_{max}(T_1)$ at wave vector (b) (k_x,k_y,k_z) in the range of temperatures 160–245 K(1), 250–475 K(2), and 480–700 K(3). The difference of waves vectors (c) $\Delta\mathbf{k}=\mathbf{k}_1-\mathbf{k}_2$ corresponding to $N_{max,1}(\mathbf{k}_1)$ and $N_{max,2}(\mathbf{k}_2)$ satisfying to relation $[1-N_{max,2}(\mathbf{k}_2)/N_{max,1}(\mathbf{k}_1)]\leqslant 0.005$.

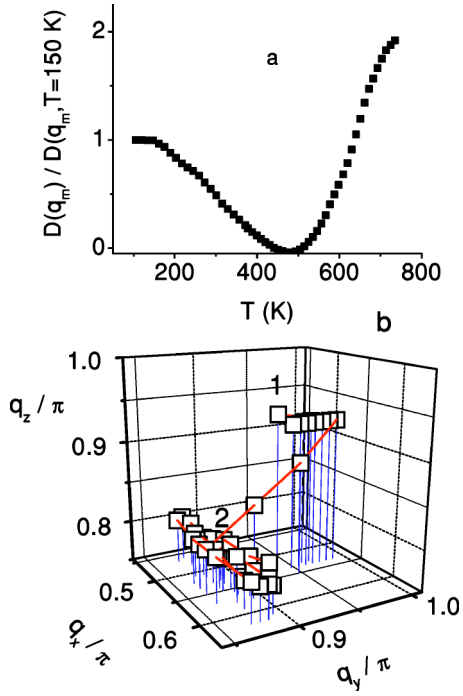

FIG. 12. The temperature dependencies of the dispersion maximal value $D(\mathbf{q_m})$ normalized to the $D(\mathbf{q_m})$ at (a) $T=150$ K and the wave vector (q_x,q_y,q_z) corresponding to (b) the largest $D(\mathbf{q_m})$, where $T=100$ K(1), 500 K(2).

crystal as shown in Fig. 1. The temperature hysteresis $\rho(T)$ observed for α-MnS (Fig. 1) should be caused by the conservation of charge ordering corresponding to rhombohedral deformation of the lattice at the temperatures above $T_1=166$ K. We suppose that the single crystal decomposes into degenerate domains with $n_\alpha \simeq n, n_\beta \to 0$. During cooling from $T\sim 500$ K in magnetic or electric field the single crystal is poling. To pass from one state to another it is necessary to overcome a potential barrier. If an external voltage V is applied to the single crystal, carrier tunnelling can be observed at the chemical potential surface. The density of states (DOS) of the single-hole excitations in the vicinity of the chemical potential $(\mu-E)\sim 0.1$ eV can be determined by voltage differentiation of current dI/dV:

$$dI/dV \propto \int_{-\infty}^{\infty} d\omega g(\omega)\frac{\partial}{\partial(eV)}f(\omega-eV)\propto g(eV). \quad (10)$$

Figure 2 presents the experimental data dI/dV, which well agree with the estimated $g(\omega)$ dependence. The small value of the negative differential resistivity within ~5% error for $V=2$ and 30 V reproduces a fine structure of the DOS near the chemical potential.

The DOS of the t_{2g} band has two maxima that allow us to understand the origin of the two maxima of the optical absorption spectra in α-MnS at $\omega\simeq 2.4$ eV and $\omega\simeq 2.9$ eV.[9] They can be ascribed to the single electron transition from the sulphur ion to the manganese ion. The line shape of the optical absorbtion is presented in Fig. 8(c) and qualitatively agrees with the DOS of the t_{2g} band. The lower band edge shows the redshift $\Delta W^{theory}\sim 0.01$ eV, $\Delta W^{exper}\sim 0.03$ eV at temperature increase from 168 to 300 K.

The location of the charges on the fixed orbitals gives rise to the orbital ordering with the wave vectors Q^{orb}_{max} closely related to the wave vector corresponding to the maximal value of $N_{max}(Q)$. As a result the orbital magnetic moments form magnetic ordering with magnetic moment $L^z(Q^{orb}_{max})=1/N\Sigma_{\mathbf{r}}\exp(-i\mathbf{r}\mathbf{Q}^{\mathbf{orb}}_{\mathbf{max}})L^z(\mathbf{r})$. Using the value of $\mathbf{Q}$ given in

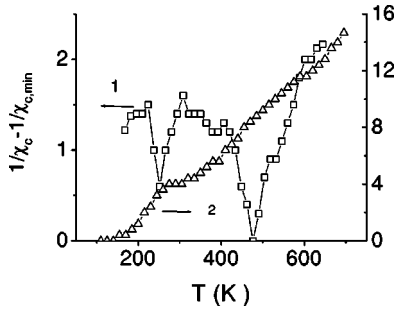

FIG. 13. The inverse value of the charge susceptibility taken from minimal value for $t_{2g}(1)$ and $e_g(2)$ bands versus temperature.

Fig. 10 at low temperatures, we obtain good agreement with experimental data. For simplicity the temperature dependence of L^z is calculated in terms of the Brillioun function with the orbital spin $L=1$. The measured and calculated values of the spontaneous magnetization are shown in Fig. 3. The minimum in the inverse value of the charge susceptibility at $T\sim 250$ K correlates with the small deviation $m^{ex}(T)$ from estimated temperature dependence $m^{th}(T)$.

The charge ordering induces the local deformation of the lattice and leads to the lowering of the local crystal symmetry that can be observed from the electron paramagnetic resonance data. The axial and rhombic terms of the single ion anisotropy D and E are determined from the temperature dependence of H_{res} using the general formula for the resonance shift due to the crystal field. The expression for the effective g value for H_{ext} applied along one of the crystallographic axes was obtained in Ref. 10:

$$\frac{g_{a,c}^{eff}(T)}{g_{a,c}} \propto 1 + \frac{D}{T - T_{\mathrm{CW}}}[(3\zeta - 1) \pm 3(1 + \zeta)\sin(2\gamma)], \tag{11}$$

where T_{CW} is the Curie-Weiss (CW) temperature; $\zeta = E/D$ and γ is the rotation angle of the MnS_6 octahedra. At $T > 200$ K the CW law of the magnetic susceptibility is satisfied and the data are described by this approach (solid lines in Fig. 5), where T_{CW} was kept fixed at 475 K, the rotation angle $\gamma=0$, $D=0.40(6)$ K, E/D is the ratio $\zeta=0.016(5)$, and the g values are $g_{[100]}=1.992(8), g_{[001]}=1.984(4)$. Our result agrees with the $D=0.34$ K value determined from antiferromagnetic resonance[11] where the gap in the magnon excitation spectrum at $\mathbf{k}=0$ was found to be equal to $\simeq 3.28$ cm^{-1}. The orbital ordering gives rise to the nonlinear behavior $\chi(T)$ in small magnetic fields. The effect of the strong irreversible change of the magnetization (Fig. 3) versus temperature at heating and cooling in the small magnetic field is explained by conservation of the degeneration of the holes in t_{2g} subbands. At the cooling in the magnetic field from temperature $T > 250$ K this degeneration is lifted and holes occupy the state with the orbital moment directed along the external magnetic field.

V. CONCLUSION

The total conductivity of MnS is the result of motion of holes in the e_g and t_{2g} bands. The holes in the e_g band are responsible for the temperature-independent behavior of conductivity at low temperatures $T < T_N$. The sharp decrease of the resistivity at $T > 200$ K is caused by the thermal activation of the holes in the degenerate t_{2g} band. The nonlinear behavior of $\rho(1/T)$ at $T > 350$ K and temperature hysteresis of the conductivity at $T < 500$ K arise from partial lifting degeneration of the holes in t_{2g} subbands observed at $250\ \mathrm{K} < T < 475$ K. The filling of two t_{2g} subbands at $T \simeq 475$ K, one of three t_{2g} subbands at $T \simeq 250$ K, and one of two e_g subbands at $T \simeq 160$ K induces the charge instability due to the competition between the on-site Coulomb interaction of the holes in the different orbitals and small hybridization of the subbands.

The localization of the charges in certain orbitals causes the orbital moment ordering and leads to the weak ferromagnetism and to the anisotropy of the g values.

ACKNOWLEDGMENTS

We thanks Professor S. G. Ovchinikov for useful discussions. This work was supported by the Russian Basic Research Foundation (REEI–BRFFI, Project No. 04-02-81018Bel2004.)

*Electronic address: apl@iph.krasn.ru

[1] M. B. Salamon and Marcelo Jaime, Rev. Mod. Phys. **73**, 583 (2001).
[2] J. S. Zhou and J. B. Goodenough, Phys. Rev. B **68**, 144406 (2003).
[3] G. A. Petrakovskii, L. I. Ryabinkina, G. M. Abramova, A. D. Balaev, D. A. Balaev, and A. F. Bovina, Pis'ma Zh. Eksp. Teor. Fiz. **72**, 99 (2000).
[4] L. I. Ryabinkina, G. M. Abramova, O. B. Romanova, N. I. Kiselev, D. A. Velikanov, and A. F. Bovina, Proceeding of the Second International Symposium, Big Sochi, Russia, OMA-II, 72 (2002).
[5] H. H. Heikens, C. F. Bruggen, and C. Haas, J. Phys. Chem. Solids **39**, 833 (1978).
[6] R. Tappero, P. Wolfers, and A. Lichanot, Chem. Phys. Lett. **335**, 449 (2001).
[7] Yu. A. Izyumov and Yu. N. Skryabin, UFN **171**, 121 (2001).
[8] I. Solovyev, N. Hamada, and K. Terakura, Phys. Rev. B **53**, 7158 (1996).
[9] O. B. Romanova, G. M. Abramova, L. I. Ryabinkina, and V. V. Markov, Phys. Met. Metallogr. **93**, 85 (2002).
[10] J. Deisenhofer, B. I. Kochelaev, E. Shilova, A. M. Balbashov, A. Loidl, and H. A. Krug von Nidda, Phys. Rev. B **68**, 214427 (2003).
[11] C. H. Perry, E. Anastassakis, and J. Sokoloff, Indian J. Pure Appl. Phys. **9**, 930 (1971).